Supplementary information for article

"Photon recycling in $CsPbBr_3$ all-inorganic perovskite nanocrystals"

Marco van der Laan[1], Chris de Weerd[1], Lucas Poirier[1+], Oscar van de Water[1], Deepika Poonia[3], Leyre Gomez[1,4], Sachin Kinge[3,5], Laurens D.A. Siebbeles[3], A. Femius Koenderink[1,6], Tom Gregorkiewicz[1†], and Peter Schall[1]*

Affiliations

[1] *Institute of Physics, University of Amsterdam, Science Park 904, 1098 XH Amsterdam, The Netherlands*
[3] *Optoelectronic Materials Section, Department of Chemical Engineering, Delft University of Technology 2629 HZ Delft, The Netherlands*
[4] *Catalan Institute of Nanoscience and Nanotechnology, CSIC, BIST, and CIBERBBN, 08193 Bellaterra Barcelona, Spain*
[5] *Materials Research & Development, Toyota Motor Europe, B1930 Zaventem, Belgium*
[6] *Center for Nanophotonics, AMOLF, Science Park 104, 1098 XG Amsterdam, Netherlands*

[+] current address: *Advanced Research Center for Nanolithography, Science Park 106, 1098 XG Amsterdam, the Netherlands*

* Email: P.Schall@uva.nl

Contents

10 pages
2 figures
1 table

[†] Tom Gregorkiewicz, July 7, 2019

1. Nanocrystal synthesis

Chemicals

Cesium carbonate (Cs_2CO_3, 99.9%), octadecene (ODE, 90%), oleic acid (OA, 90%), oleylamine (OLA, 70%), lead(II) bromide ($PbBr_2$, 98%), toluene (ACS reagent ≥99.5%). All chemicals were purchased from Sigma-Aldrich and were used with no further purification, except for the drying period reported in the IP-NC synthesis procedure.

Synthesis of nanocrystals

$CsPbBr_3$ NCs were synthesized following the protocol reported by Protesescu *et al.* with some modifications.[1] Briefly, 30 mL of ODE and 1.88 mmol of $PbBr_2$ were exposed at 120 C for 1h under N_2. Then, 10 mL of dried OLA and OA (1:1 volume ratio) were added and the temperature was set to 160 °C. After complete dissolution of the lead salt, 4 mL of warm Cs-oleate solution were injected. The reaction took place for 5 seconds and the flask was immediately cooled down with an ice-water bath. The product was purified by multiple cycles of centrifugation and redispersion in toluene. The Cs-oleate solution was prepared by stirring 0.814 g of Cs_2CO_3 with 40 mL of ODE and 2.5 mL of OA at 150 °C under N_2 atmosphere; all reactants were dried beforehand. The final product, which has been used as the initial sample for the study, referred to as Dilution 1, had a concentration of 85 mg/mL. Further dilutions were prepared by adding the appropriate amount of toluene.

2. Random Walk Simulations

Simulations of the scattering, absorption and re-emission processes were performed based on photon walks through the dispersion of nanocrystals at various concentrations, in two dimensions. In these simulations, a single random walk is initiated by a photon that is initialized in a two-dimensional square cuvette with wavelength (λ), at position (x,z) and in some random direction (θ), see figure S1A, with an initial spatial distribution reflecting the pencil shaped excitation in our experiment, and wavelength drawn from the emission spectrum of the most diluted sample. This photon then travels ballistically through the cuvette between absorption-re-emission events, where a new random propagation direction is drawn. The mean distance between these events is set by the optical mean-free path length, while re-emission is governed by the photoluminescence quantum yield (PLQY) and the photon wavelength gains an offset determined by the Stokes shift. At the cuvette boundaries, photons can either escape or be reflected as described by the Fresnel equations. One of the four walls of the cuvette corresponds to the detector plane, where the wavelength of the detected photon is recorded, while the other boundaries are open for photons to escape the simulation without being recorded on a detector, mimicking the open boundaries of the experiment. All these processes, and the initialization values (x, λ, θ), are described in the simulation by probabilities. By iterating the simulation over 10^6 photons, a probability distribution of detected photon wavelengths is constructed, one for each set of the experimental variables, i.e. distance *z* between excitation and detection positions, and specific nanocrystal dilution. In the following, we give more details of these processes, and explain their connection to experimental parameters.

2.1 Step-size

A photon travelling through the dispersion interacts with the nanocrystals by scattering or absorption, the latter followed by eventual re-emission. The distance between these events is set by the mean free path $l_{mfp}(\lambda)$ which depends on the concentration of nanocrystals in the suspension, and their scattering and absorption cross sections, and can be determined from transmission measurements as follows

$$T_L(\lambda) = \frac{I_L(\lambda)}{I_0(\lambda)} = e^{-\mu(\lambda) * L} \quad \text{(S1a)}$$

$$l_{mfp}(\lambda) = \frac{1}{\mu(\lambda)} \quad \text{(S1b)}$$

Here, $T_L(\lambda)$ is the wavelength-dependent transmittance of a beam of light with intensity $I_L(\lambda)$ after traveling a distance L through the suspension, given the initial intensity I_0. The Beer-Lambert law (S1a) states that the intensity of light drops exponentially over distances with the material-specific attenuation coefficient, $\mu(\lambda)$. The inverse of this attenuation coefficient defines the mean-free-path length, l_{mfp} (λ) (S1B). We determined l_{mfp} (λ) for all nanocrystal dilutions from the measured transmittance spectra of the diluted nanocrystal samples. This mean-free-path sets the average step size in the simulations.

2.2 Reflection

When encountering the boundaries, the diffusing photon can leave the cuvette, or be reflected off the walls, with incident angle-specific probabilities determined by the Fresnel coefficients as follows:

$$R_s = \left| \frac{n_1 \cos(\theta_i) - n_2 \sqrt{1 - \left(\frac{n_1}{n_2}\sin(\theta_i)\right)^2}}{n_1 \cos(\theta_i) + n_2 \sqrt{1 - \left(\frac{n_1}{n_2}\sin(\theta_i)\right)^2}} \right|^2$$

$$R_p = \left| \frac{n_1 \sqrt{1 - \left(\frac{n_1}{n_2}\sin(\theta_i)\right)^2} - n_2 \cos(\theta_i)}{n_1 \sqrt{1 - \left(\frac{n_1}{n_2}\sin(\theta_i)\right)^2} + n_2 \cos(\theta_i)} \right|^2 \quad (S2)$$

$$R_{eff} = \frac{1}{2}(R_s + R_p)$$

Here R_s and R_p are the Fresnel equations for light travelling under incident angle θ_i, from a material with refractive index n_1 towards a material with refractive index n_2, for s and p polarizations, respectively. Under the assumption of unpolarized light, the effective Fresnel coefficient R_{eff}, indicating the probability of reflection, is the simple average of the s and p components. In principle, R_{eff} is wavelength-specific by virtue of the wavelength dependence of the refractive indices.

2.3 Scattering, absorption and re-emission

The probability of scattering and absorption are determined by the respective cross sections, which are not known a priori. In principle, these cross-sections can be determined analytically from the work of Zijlstra et al.[2]; however, this would rely on assumptions. We therefore took advantage of the measured transmission spectra to back out the absorption- and scattering probabilities from measurements, as detailed in 1.5 below. Furthermore, in case the photon is absorbed, the probability of re-emission is 0.9, as given by the experimentally determined photoluminescence quantum. Upon re-emission, a photon's wavelength is red-shifted by the so-called Stokes shift. While we have an ensemble measure of the Stokes shift from the difference in wavelength between absorption onset and the PL peak of the nanocrystal suspension, it is not so clear, what the Stokes shift of a single nanocrystal is and how it depends on the nanocrystal size and its absorption/emission wavelength. We therefore used this Stokes shift as a free adjustable parameter and establish its magnitude by the approach outlined below.

2.4 Termination of the simulation

A single simulation run of a diffusing photon is finished when the photon has either escaped through the cuvette boundaries, is absorbed without re-emission, or has been detected at the detection boundary with an angle of ± 0.1 radians. The latter is specified to model the actual detection geometry of the experimental setup, where a finite-size collection lens captures the photons incident within an angular range of ± 0.1 radians and projects them onto the detector. Table S1 summarizes all relevant inputs to the model.

	Experiment	**Simulations**
Cuvette Dimension	3D	2D
Cuvette Size	10 x 10 x 35 mm	10 x 10 mm
Initialization	Excitation by 490 nm laser	After first emission event. Photon wavelengths randomly chosen from experimental "Recycling-Free" PL spectrum
Laser spot diameter	~ 0.5 mm	Infinitesimal
Excitation penetration depth	Determined by Beer-Lambert law.	Assumed constant over the width of the cuvette
# of Photons	-	10^6
Dilution Factors	2, 5, 10, 25, 50	2, 5, 10, 25, 50
Distances	0.5 to 8 mm in steps of 0.5 mm	0 to 7 mm in steps of 1 mm
s, p polarization $CsPbBr_3$ PL	Unpolarized	Unpolarized, equal weight
n_1, n_2 refractive indices	Toluene, quartz, air	Toluene (1.4968)[3], air (1)[3]
Absorption / Scattering coefficients	-	*See figure S1*
Photoluminescence Quantum Yield	0.9	0 *(Recycling OFF)* 0.9 *(Recycling ON)*
Stokes shift	-	4 nm

Optical path length distribution	-	Gaussian *Mean:* mfp length *Width:* 0.5 x mfp length
Detection path	> 1 m	**Angle restriction:** $-0.1\ \text{rad} < \theta < 0.1\ \text{rad}$

Table S1*:* Comparison between experimental and simulation details.

2.5 Determination of model parameters

In order to best calibrate the simulations with the experiments, we determine and refine the main parameters, i.e. the mean-free-path length, the corresponding optical path length distribution width and the Stokes shift from experimental measurements and their extrapolation. In particular, we use the expected linear relation between the mean-free-path length and the nanocrystal dilution to correct the mean-free-path length and determine the relative contribution of scattering versus absorption.

2.5.1 Reflection

The Fresnel equations are assumed to be wavelength independent over the narrow wavelength range of interest (475 – 550 nm), e.g., the refractive indices are assumed to be constant over wavelength. We assume specular reflection on the walls of the cuvette. After reflection on the walls the photon travels the remaining portion of its pre-determined mean-free-path length before entering the next iteration in the simulation.

2.5.2 Mean-free path length

We use eq. (S1b) to obtain the mean-free-path length from the attenuation coefficient determined from transmission measurements. The thus determined mean-free-path length shows some saturation behaviour for short wavelengths and low-dilutions, see figure S1B. We associate the saturation behaviour in this strongly absorbing case with the low number of detected photons, which becomes of the order of the detector sensitivity. To correct for it, we use linear extrapolation of the data towards lower dilution, see solid blue and dark green lines in figure S1B. We apply this correction specifically for wavelengths shorter than 510 nm, the absorption edge. For longer-wavelength light in contrast, absorption effects vanish, scattering contributes increasingly to the light-nanocrystal interaction. This scattering leads to a reduction of the mean-free-path lengths with respect to that based on absorption alone, as shown by the dashed green and orange curves in Fig. S1b. We use this deviation of the mean-free path curves from the simple linear relationship in the case of absorption to determine the relative contribution of absorption and scattering. The absorption-versus-scattering probability can be estimated from the ratio of the dashed curves and the extrapolated lines, as described by,

$$P_{abs} \approx \frac{mfp_{dashed}}{mfp_{corrected}} \qquad \text{(S3a)}$$

$$P_{abs} \approx \frac{\mu_{abs}}{\mu_{abs} + \mu_{scat}} \qquad \text{(S3b)}$$

Here, we assume that the single-photon absorption probability can be estimated by taking the ratio of the two described curves, for wavelengths longer than the absorption onset. This estimate relies on the assumption that the corrected curve is dominated by absorption and through equation S1b, substituting the sum of absorption and scattering coefficients for μ, we see that the absorption probability is approximated as in equation S3b.

The probability of scattering is then one minus this absorption probability. Scattering is always assumed to be elastic in the model, e.g. photons do not undergo a change in wavelength.

We have chosen a Gaussian distribution of free path lengths with mean equal to the mean-free path length as determined from the transmittance spectra, and adjustable width, which can be calibrated using the experimental transmittance spectra. To do so, we simulated the transmittance spectra for a range of wavelengths and nanocrystal dilutions, using the same photon diffusion process as described above, and compared the resultant simulated transmittance with the experimentally measured one, as shown in figure S1C. Reasonable agreement for all dilutions is obtained for a relative width of 0.5 times the mean-free-path length, which we have chosen for the simulations.

2.5.4 Stokes shift

The Stokes shift is a crucial parameter as it affects the number of re-emission cycles as well as the red-shift of the photoluminescence peaks. While we know the ensemble Stokes shift from the wavelength separation of the absorption edge and the PL peak of the ensemble spectra, the value for the individual nanocrystals is not exactly known. We therefore optimized this value by comparison of the simulated and experimentally measured PL spectra.

We ran the simulations for various Stokes shift values (2-5 nm) and compare simulations with re-emission turned on and re-emission turned off with the experimental trends. This comparison, shown in Fig S1D, clearly establishes that the Stokes shift parameter has a significant effect on the center wavelengths of simulated photoluminescence peaks. Nevertheless, for all chosen Stokes shift values, the center wavelengths with re-emission on consistently approximate the experimental center wavelengths better than the center wavelengths with re-emission-off, demonstrating that re-emission is a necessary process to reproduce the experimental trends.

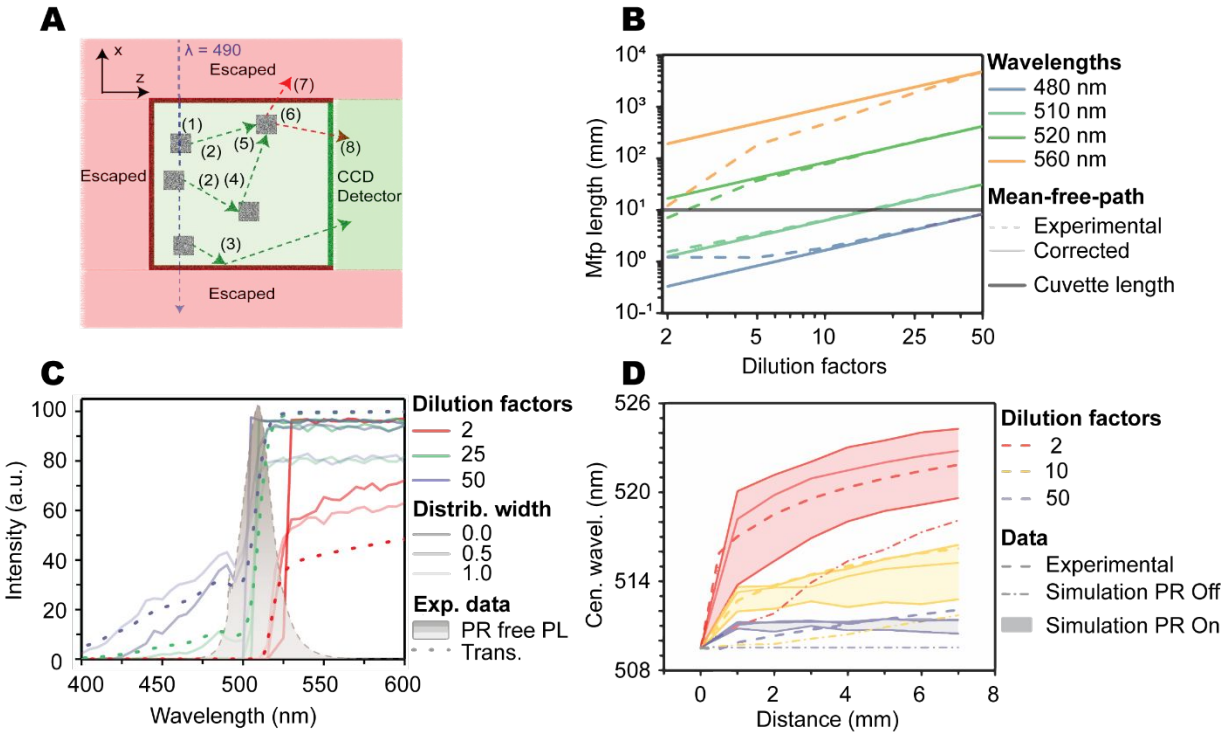

Figure S1. *Simulation details and results.*

A) *Schematic of the simulation. After initial excitation (1), nanocrystals emit photons (2) that then travel a distance of around the mean-free-path length. Subsequently, they can be reflected off the cuvette walls (3), scattered (4) or re-absorbed by other nanocrystals (5). After re-absorption, photons can be re-emitted (6) and this cycle can happen multiple times until the photon either escapes (7) or is detected (8).* ***B)*** *Mean free path lengths as a function of dilution factor (log-log scale). Color indicates photon wavelength. Dashed and solid lines indicate, respectively, mean-free-path lengths determined from experimental transmittance spectra, and correction by linear extrapolation to low dilution, as discussed in section 1.5.3.* ***C)*** *Experimental (dotted) and simulated (solid) transmittance spectra for various dilutions (color) and different values for the optical path length distribution width (shading). The beige PL spectrum is included to show the overlap of the transmittance spectra with the experimental PL spectrum of the most diluted sample closest to the detector. Based on these simulations a distribution width factor of 0.5 was chosen as most optimal.* ***D)*** *Center wavelengths of experimental (dashed) and simulated photoluminescence spectra (solid lines and shade) for dilution factors 2 (red), 10 (yellow) and 50 (purple). The shaded regions indicate simulation results for Stokes shift values from 2 (lower bounding curve) to 5 nm (upper bounding curve), with a Stokes shift value of 4 nm (value used in the manuscript) indicated as slightly faded solid line in between. Simulation results with re-emission turned off are shown as dash-dotted lines; they are far below the experimental measurements. Thus, while the range of Stokes shift values result in a significant spread in center wavelengths, photon recycling has to be involved to describe the trends observed in experiments.*

3. Time-resolved photoluminescence measurements

The time-resolved photoluminescence (TRPL) measurements were carried out in time-correlated-single-photon counting (TCSPC) mode with a LifeSpec ii system from Edinburgh Instruments coupled to a VIS PMT detector and with a 375 nm pulsed diode laser as an excitation source. As in the other experiments, the nanocrystals were dispersed in toluene in various concentrations and kept in 3.5 mL quartz cuvettes. These samples were excited in the back of the cuvette, furthest from the detector, to allow for multiple possible recycling events.

The fitting of all the TRPL data was done with a phenomenological function, shown in equation S4, that separates the rise and decay parts of the histograms.

$$for\ t < t_c: \qquad y = y_0 + \frac{A_1}{1 + e^{-\frac{t - \frac{t_c}{2}}{t_r}}} \qquad (S4)$$

$$for\ t \geq t_c: \qquad y = y_0 + A_1 * e^{-\frac{t - t_c}{t_d}}$$

In this fitting function t_c is the time where the TRPL data peaks with amplitude A_1 above a baseline of y_0. Then, the parameters t_r and t_d denote the rise and decay parameters, respectively. For times t before t_c the data is fitted by a sigmoid function while after this characteristic time the data is fitted with a single exponential decay. The extracted rise and decay times are shown, respectively, in Fig. 4B and C of the main text.

4. Various photoluminescence spectra

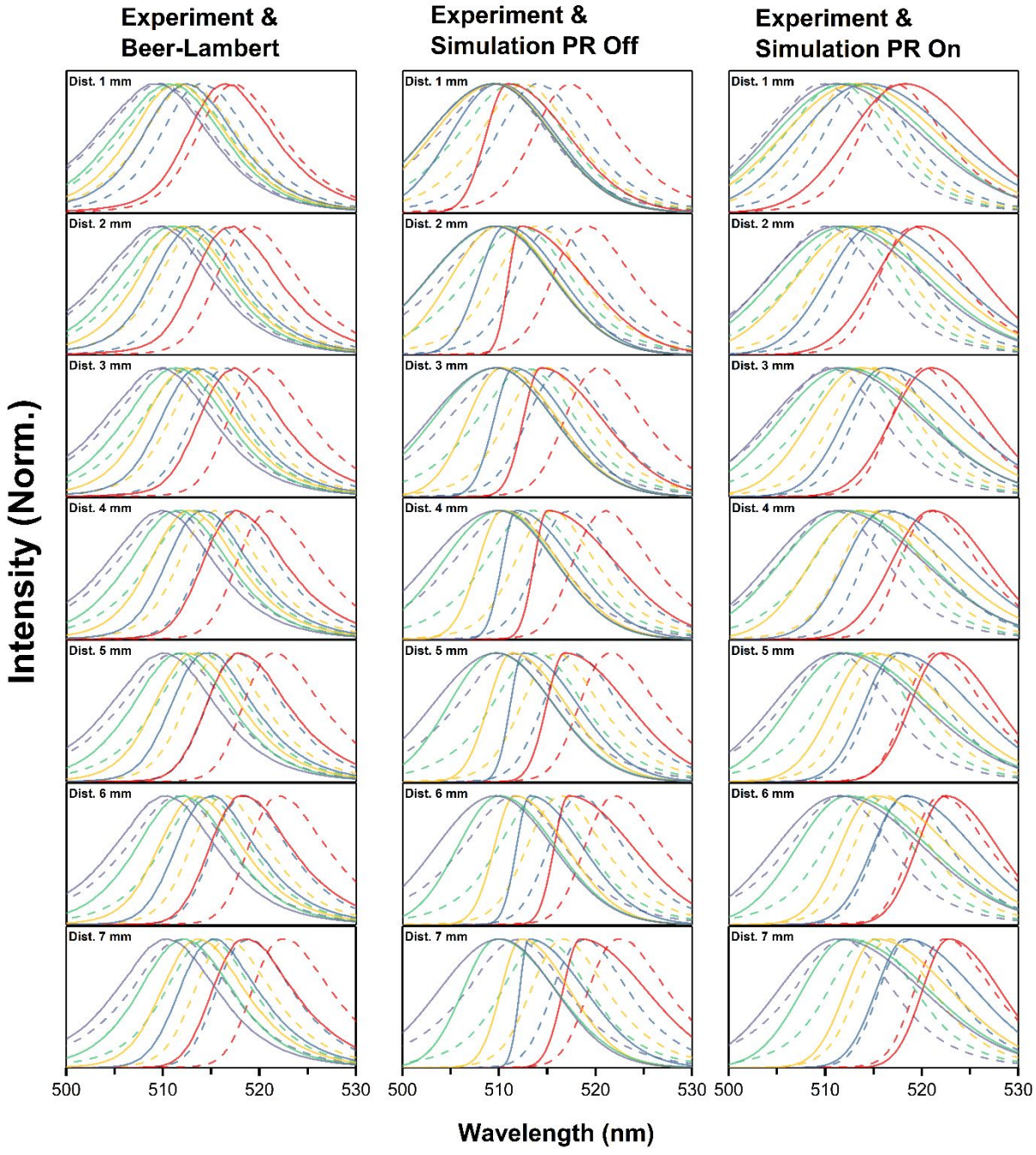

Figure S2. *Comparison of experimental data (dashed) with differently modelled spectra (solid): modelled by the Beer-Lambert law (left), modelled by simulations with re-emission turned off (middle) and by simulations with re-emission turned on (right). Colour indicates dilution factor 2 (red), 5 (blue), 10 (yellow), 25(green) and 50(purple) and rows indicate various excitation-detector distances, increasing from top to bottom.*

5. Estimation of Brownian motion

As the nanocrystals are well dispersed and exhibit diffusion, there might be some other type of transfer happening between them. We estimate the occurrence of such transfer based on Brownian motion by using the Stokes-Einstein relation to determine the average distance $\overline{x}$ a single nanocrystal travels within the carrier lifetime according to [4]

$$D = \frac{k_B T}{6\pi \eta r} \qquad \text{(S5a)}$$

$$\overline{x} = \sqrt{6\, D\, \tau} = \sqrt{\tau \frac{k_B T}{\pi \eta r}} \qquad \text{(S5b)}$$

where, τ is the elapsed time, k_B and T (293 K) are the Boltzmann constant and temperature respectively, η is the viscosity of the solvent (toluene, 0.55 x 10^{-3} Pa*s)[5] and r is the radius of the particles. We assume that the nanocrystals are spherical with a radius of r=5 nm, corresponding to half the edge length of the 10 nm cubes, and take τ =10 ns to be the PL decay time. This results in an average displacement due to Brownian motion of around 2nm equivalent to a possible interaction volume of around 35 cubic nanometers.

The nanocrystal concentration of the stock solution of these samples, determined from the mass fraction of 85 mg/mL, using the density of bulk $CsPbBr_3$ perovskite of 4.86 g/cm^3 [6] and the average size of around 10 nm, is 17.5 x 10^{-6} nanocrystals per cubic nanometer, almost six orders of magnitude smaller than the density needed for sufficient interaction based on Brownian motion. Hence, even in the most concentrated sample, the nanocrystal density is simply too small to allow for a significant amount of nanocrystal diffusion-based transfer processes. In addition, the PL rise-time clearly favours a transfer process with a rate similar to the effective rate obtained from the PL decay dynamics, indicating radiative transfer. All of this combined, we exclude any significant contribution from other transfer mechanisms such as carrier-diffusion or Förster resonance energy transfer in the observed spectroscopic features.

6. References

[1] Protesescu, L., Yakunin, S., Bodnarchuk, M.I., Krieg, F., Caputo, R., Hendon, C.H., Yang, R.X., Walsh, A. and Kovalenko, M.V., 2015. Nanocrystals of cesium lead halide perovskites (CsPbX3, X= Cl, Br, and I): novel optoelectronic materials showing bright emission with wide color gamut. Nano Lett., 15(6), pp.3692-3696.

[2] Zijlstra, P., Orrit, M. and Koenderink, A.F., 2014. Metal nanoparticles for microscopy and spectroscopy. In Nanoparticles (pp. 53-98). Springer, Berlin, Heidelberg.

[3] Kedenburg, S., Vieweg, M., Gissibl, T. and Giessen, H., 2012. Linear refractive index and absorption measurements of nonlinear optical liquids in the visible and near-infrared spectral region. Opt. Mater., 2(11), pp.1588-1611.

[4] Einstein, A., 1905. Über die von der molekularkinetischen Theorie der Wärme geforderte Bewegung von in ruhenden Flüssigkeiten suspendierten Teilchen. Ann. Phys., 4.

[5] Santos, F.J., Nieto de Castro, C.A., Dymond, J.H., Dalaouti, N.K., Assael, M.J. and Nagashima, A., 2006. Standard reference data for the viscosity of toluene J. Phys. Chem. Ref. Data, 35(1), pp.1-8.

[6] Liu, Z., Peters, J.A., Stoumpos, C.C., Sebastian, M., Wessels, B.W., Im, J., Freeman, A.J. and Kanatzidis, M.G., 2013, September. Heavy metal ternary halides for room-temperature x-ray and gamma-ray detection. In Hard X-Ray, Gamma-Ray, and Neutron Detector Physics XV (Vol. 8852, p. 88520A). International Society for Optics and Photonics